Desalination and Water Treatment
www.deswater.com

doi: 10.5004/dwt.2022.28036

247 (2022) 258–271
January

Application of machine learning methods to removal percentage prediction for Malachite green adsorption on kaolinite

Murat Canayaz[a], Adnan Aldemir[b,c,*], Ali Rıza Kul[d]

[a]*Faculty of Engineering, Computer Engineering Department, Van Yüzüncü Yıl University, 65080, Van, Turkey, email: mcanayaz@yyu.edu.tr*
[b]*Faculty of Engineering, Chemical Engineering Department, Van Yüzüncü Yıl University, 65080, Van, Turkey, email: adnanaldemir@yyu.edu.tr*
[c]*Faculty of Engineering, Mechanical Engineering Department, Van Yüzüncü Yıl University, 65080, Van, Turkey*
[d]*Faculty of Science, Chemistry Department, Van Yüzüncü Yıl University, 65080, Van, Turkey, email: alirizakul@yyu.edu.tr*

Received 10 August 2021; Accepted 11 December 2021

ABSTRACT

In this study, the removal percentage was estimated using machine learning methods, such as artificial neural network, radial basis function neural network, support vector regressor, and random forest regressors, for data obtained during Malachite green adsorption on kaolinite as an adsorbent in an aqueous solution. Important process parameters, including initial dye concentration, sonication time and temperature, were investigated. Statistical evaluation metrics such as R^2, mean squared error, and root mean square error were used to evaluate the performance of the models. Among these models, the artificial neural network was more successful compared to other models with 0.98 R^2 values for three temperatures. Radial basis function neural network and random forest regressors were observed to achieve successful results. In this study, the results obtained from the machine learning methods are given comparatively. The initial dye concentrations increased from 10 to 60 mg L^{-1}, the removal percentage of Malachite green on kaolinite increased from 68.71% to 79.61% for 298 K, 72.26% to 82.58% for 308 K and 78.75% to 85.91% for 318 K, respectively. Isotherm, kinetic and thermodynamic calculations for Malachite green removal by kaolinite were completed. The equilibrium of Malachite green adsorption onto kaolinite was best described by the Langmuir isotherm and the kinetics of the process followed the pseudo-second-order model, which had the highest correlation values. Thermodynamic analysis of experimental data suggests that the adsorption process is spontaneous and endothermic in nature.

Keywords: Adsorption; Machine learning; Artificial neural network; Malachite green; Kaolinite

1. Introduction

Water resources are limited and they are decreasing with the increase in world population. Wastewater, in which the most important pollutants are dyes and heavy metals, is increasing with the growth of industry [1,2]. In recent years, treatment of dyes in wastewater has become important for the solution of environmental problems caused by high toxicity. Dyes are used in various industries and even very low concentrations of dyes in wastewater discharged from these industries is undesirable because of the negative effect on life [3,4]. Dyes have complex aromatic molecular structures that make them stable and resistant to biodegradation, light and oxidizing agents. The dyes in wastewater consume soluble oxygen under chemical and biological conditions and endanger the life of aquatic animals due to their toxicity [5–7]. The prolonged accumulation of dyes in the human body causes several

* Corresponding author.

diseases and disorders such as allergies, fever, dermatitis, rashes and cancer. So, dye removal from wastewater before it pollutes non-contaminated water is important [8,9]. Different methods have been proposed for removal of dyes from wastewater. Coagulation, flocculation, photocatalytic degradation, membrane filtration, microbiological decomposition, electrochemical oxidation and adsorption are the most commonly-used methods [10–12]. The advantages of adsorption which make it suitable for water pollution control include: less investment in terms of initial costs, simple design, easy operation, less energy requirements and lack of hazardous by-products [13,14].

Using an efficient adsorbent plays a key role in the adsorption process. During the past decades, many adsorbents have been prepared for dye removal from wastewater [15–17]. Among these adsorbents, clays contain exchangeable ions on their surface, which can adsorb cations and/or anions. Furthermore, they are cheap, abundant in nature and have high surface area [18]. It is well known that kaolinite is composed of silicate sheets and gibbsite layers with heterogeneous surface charge. It is believed that its surface has a structural charge and adsorption can occur on flat exposed planes of silica and alumina sheets. Kaolinite has no side effects and no health problems if fine dust particles are controlled, so it is environmentally safe Apart from industrial applications, kaolinite may be used for environmental remediation and wastewater treatment alongside other clays [19]. Malachite green (MG) dye was chosen as the adsorbate in this study due to its industrial applications and also use as an antiparasitic agent in aquaculture to prevent parasitic worm infections in fish gills and eggs [20,21]. Besides its industrial use, MG has toxic properties as it can bioaccumulate in organs such as liver, kidney, muscle and skin. MG was also verified to possess mutagenic and carcinogenic properties [22]. Therefore, it is necessary to treat wastewater containing MG.

In recent years, various methods have been used to estimate the adsorption process in chemical events. Artificial neural network (ANN), radial basis function neural network (RBFNN), support vector regressor (SVR), random forest regressor (RFR), adaptive neuro-fuzzy inference system (ANFIS), and support vector machine (SVM) methods were used in these studies for modeling and simulation. The SVR method was used to predict the Ni(II) ion removal efficiency during adsorption by Parveen et al. [23]. Ahmadi Azqhandi et al. [24] used machine learning techniques such as RBFNN and RFR for the modeling and optimization of ultrasonic-assisted adsorption of bright green on ZnS-NP-AC. In the study conducted by Mahmoodi et al. [25], the least squares support vector machines (LSSVM) method was applied to model the data. In another study using machine learning methods such as RBFNN and multilayer perceptron (MLP), Tayebi et al. [26] used these methods to estimate adsorption values for reactive orange 16 removal. Yildiz [27] benefited from the ANN method in his study about adsorption of Zn(II) ions in aqueous solutions onto peanut shells.

In this study, the machine learning methods of ANN, RBFNN, SVR, and RFR were trialed to estimate the removal percentage value resulting from the use of MG as an adsorbate. Initial concentration of dye, interaction time and temperature were considered the input data and the removal percentage of MG was calculated as the output data for the applied machine learning methods. This study will contribute to the literature as it is the first time that different machine learning methods have been compared to estimate the removal percentage for adsorption of MG dye on kaolinite. Also, this study aimed to predict the adsorption performance of kaolinite for MG dye removal from aqueous media in terms of isotherm, kinetic and thermodynamic calculations.

2. Materials and methods

2.1. Adsorbent

The kaolinite sample KS 1 (Ukraine) was obtained from Eczacıbaşı Co. in Turkey. The chemical constituents of kaolinite were observed as follows; 48.39% SiO_2, 35.99% Al_2O_3, 0.43% Fe_2O_3, 0.58% TiO_2, 0.24% CaO, 0.09% MgO, 0.03%, Na_2O, 1.74% K_2O and 12.39% loss on ignition. The pore-size distributions, X-ray diffractograms and the cation-exchange capacities of the kaolinite samples were determined. Details of the adsorption events based on characterization results were given in previous publications by the authors [28,29].

2.2. Adsorbate

In this study, Malachite green (basic green, aniline green, fast green), which is a water-soluble dye belonging to the triphenylmethane family, was used in experiments. MG oxalate was used as the adsorbate in the current research. The formula of MG is $C_{52}H_{54}N_4O_{12}$ (MW 927.01 g mol^{-1}) and it was obtained from Merck Chemical Company. A stock solution was prepared by dissolving the required quantity of MG in distilled water. The solutions with required concentration used for the adsorption process were prepared by diluting the stock solution of MG with deionized water. Different dye concentrations (10, 20, 40, 60 mg L^{-1}) of MG were prepared using the stock dye solution. All other reagents used were of analytical grade and used without purification.

2.3. Batch adsorption experiments

In the adsorption experiments, which were carried out in a temperature-controlled water bath, 1 g kaolinite was treated with 500 mL of dye solution. Temperature was kept constant within ±0.2°C. The MG concentration in the dye solution was determined over 220 min. The same processes were carried out at temperatures of 298 K, 308 K and 318 K. Each experiment was conducted in triplicate and the average of the obtained data was taken as the result.

The concentration of MG in solution at maximum absorbance wavelength of 617 nm was evaluated using an ultraviolet-visible (UV/VIS) spectrophotometer (PG Instruments Ltd., T80 model). A calibration curve was prepared by plotting absorbance and various dye concentrations. Unknown MG concentration was determined with the calibration curve. The equilibrium adsorbent capacity (q_e) for MG was found using Eq. (1):

$$q_e = \frac{\left(C_0 - C_e\right) \times V}{m} \tag{1}$$

where V is the solution volume (L), C_0 is the initial concentration of the dye (mg L^{-1}), C_e is the equilibrium concentration of the dye (mg L^{-1}) and m is adsorbent mass (g). The dye removal percentage was calculated using Eq. (2):

$$\text{Removal percentage}\left(\%\right)=\frac{C_0-C_t}{C_0}\times 100 \tag{2}$$

The effects of the initial dye concentration, temperature and contact time on the adsorption of MG were investigated with machine learning methods. The effect of initial dye concentration, which is one of the most important parameters driving adsorption, was studied by varying initial concentrations of dye solution for adsorption by kaolinite in the range of 10–60 mg L^{-1} and the temperature effects on the equilibrium of MG adsorption on kaolinite were determined at 298 K, 308 K and 318 K.

2.4. Application of machine learning methods

2.4.1. Artificial neural network

ANN is an information processing tool that aims to fulfill the functions of learning, associating, classifying, generalizing, predicting, and feature determination based on the nervous systems in living creatures. ANNs are nonlinear statistical models that use a complex relationship between inputs and outputs to find a new model. The building blocks of ANN are artificial nerve cells. There are five basic parts which consist of inputs, weights, addition function, activation function and outputs. The inputs are determined by the samples that the network sends to the artificial nerve cell, which it is then asked to learn. Weights show the importance of the information coming to an artificial cell and its effect on the cell. The sum function calculates the net input to a cell. The activation function processes are the net input to the cell and determine the output that the cell will produce in response to this input. The output is the output value determined by the activation function. Artificial nerve cells produce their output by evaluating the inputs given to them according to the weight of each input. ANN transmits the data it receives from the input layer to the output layer by processing it in the intermediate layers. The margin of error is calculated by comparing the output with the expected output for each input in the training set. This margin of error is transmitted back in proportion to the weights that connect the neurons between the output layer and the input [30,31]. The network structure used for our application consists of three layers; input, hidden layer and output. The input values are initial dye concentration, contact time, temperature, and the output value is the removal percentage. The simple ANN structure used for our application is given in Fig. 1.

2.4.2. Radial basis function neural networks

This network structure, which is an alternative to artificial neural networks, has three layers. These are the input, hidden and output layers. Unlike ANN, activation functions called RBF are used between the input layer and hidden layers. In addition to being trained in a shorter time compared to ANN, they have begun to be used as an alternative network to ANN because they are not stuck to the local minimum. In these networks, inputs are transmitted directly to the hidden layer without being multiplied by their weight values. In the hidden layer, a series of radial based functions are applied to the inputs and sent to the output layer. Each RBF function has two parameters that define the center of the function and its standard deviation [32]. A commonly used radial basis function is the Gauss function. The RBFN network architecture, whose input is defined as x and output as $y(x)$, using the Gauss function is defined with Eq. (3).

$$y\left(x\right)=\sum_{i=1}^{M}w_i\exp\left(-\frac{\left(\left\|x-c_i\right\|\right)^2}{2\sigma^2}\right) \tag{3}$$

where c_i is called center and σ is called standard deviation. There are M basic functions with c_i center and w_i are weights in the functions. Activating the hidden layer is determined by the distance between an input vector x and the center of the function. In cases where these parameters are close to each other, high activation is achieved. Then, by calculating the interpolation matrix, weights between the input layer and the output layer are found. The purpose of training RBFN networks is to find c_i centers and w_i weights. The RBFNN structure is shown in Fig. 2 [33].

2.4.3. Random forest

Random forest (RF), which is a supervised machine learning algorithm, tries to obtain estimation values from

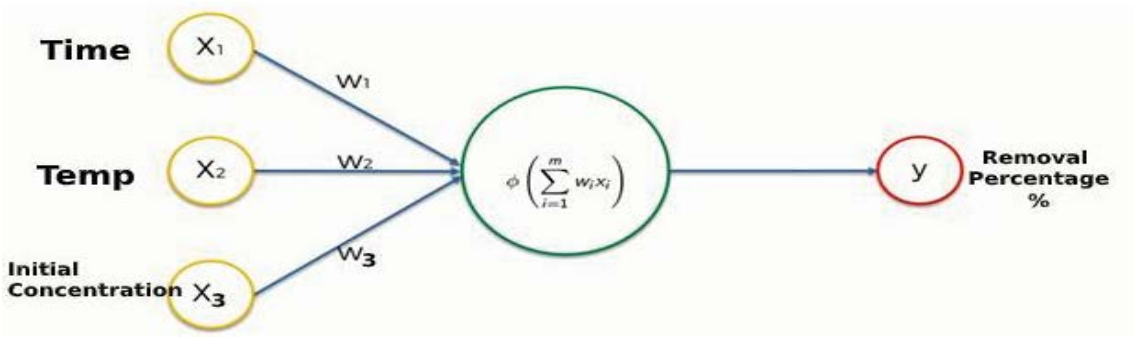

Fig. 1. Artificial neural network structure.

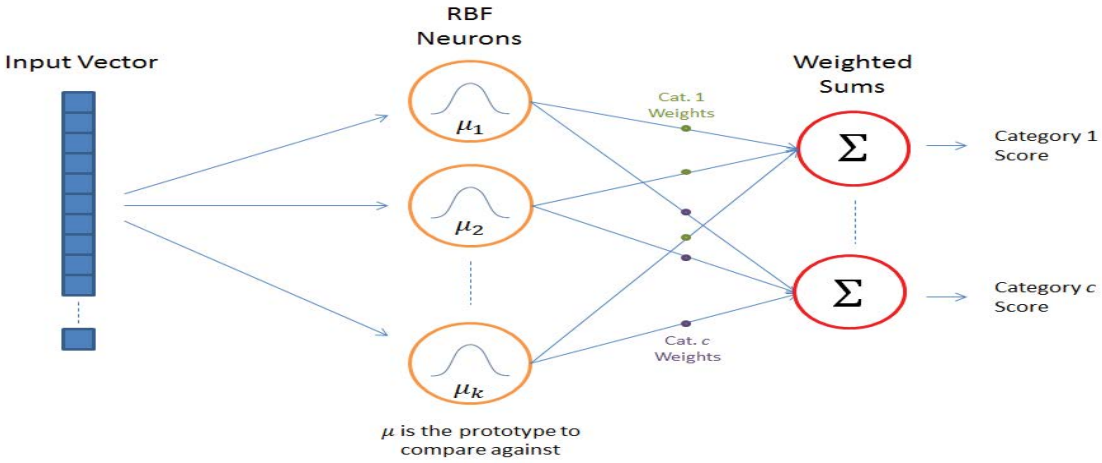

Fig. 2. Radial basis function neural network structure.

decision trees selected with the bagging method. It has an important place among machine learning algorithms as it is used for both classification and regression problems. The importance of each feature in the dataset to be used in this algorithm can be measured relatively. Considering the importance of the feature, the features affecting the prediction can be reserved and unnecessary features can be reduced. There are some important hyper parameters used in this algorithm. The first one is the number of trees that will be found in the forest. Another parameter is the maximum number of features allowed for a tree called max_features. Another parameter that may be important is the min_sample_leaf parameter, which determines the minimum number of leaves required to separate an inner node [34]. The working principle of the RF algorithm can be summarized as follows and is shown in Fig. 3.

Step 1: First, random samples are selected from a particular dataset.

Step 2: A decision tree is created for each selected sample. Each decision tree is taken from the predicted result.

Step 3: Voting is made for each predicted result.

Step 4: The prediction with most votes is selected as the final prediction.

2.4.4. Support vector regressor

SVR is one of the best-known algorithms for regression problems. Unlike SVM, its output is used to find the most suitable hyper plane for problems consisting of real numbers. SVR has good generalizing capacity. Therefore, high prediction accuracy is achieved. The computational complexity of SVR is independent of the size of the input space which gives SVR an important advantage [35,36]. The following equation is used for the mathematical formulation of SVR. The SVR structure is shown in Fig. 4.

$$\text{minimize}\ \frac{1}{2}\|w\|^2 + C\sum_{i=1}^{n}\left(\xi_i^* + \xi_i\right)$$

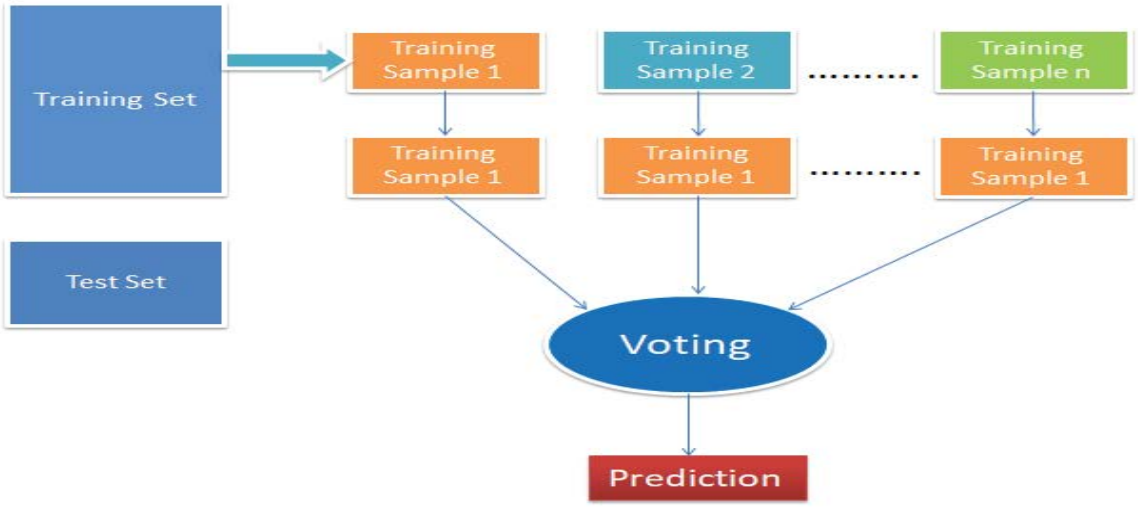

Fig. 3. Random forest structure.

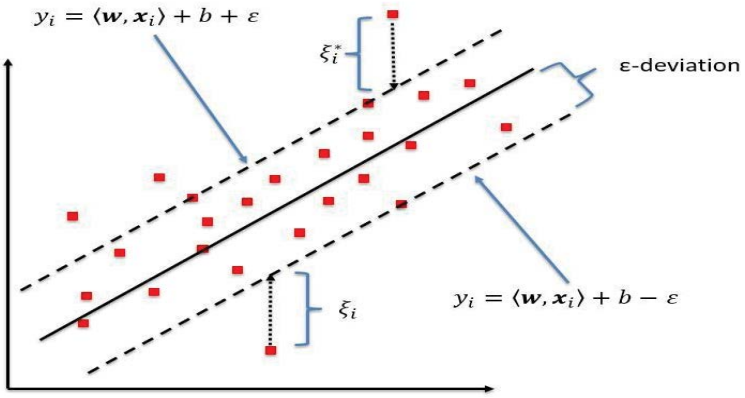

Fig. 4. Support vector regressor structure.

$$\text{subject to} \begin{Bmatrix} y_i - \langle w, x_i \rangle - b \le \epsilon + \xi_i^* \\ \langle w, x_i \rangle + b - y_i \le \epsilon + \xi_i \end{Bmatrix} \tag{4}$$

where w is weight vector, x_i is i-th input value, y_i is training data label, and ξ_i is the distance between the estimated value outside the limit and the limit. C is a parameter used to keep the values out of bounds.

A series of mathematical functions are used in SVR to convert the data it receives as input, called the kernel, into the required form. Nonlinear predictions can be made in the model created by these kernel functions. In our study, linear, polynomial and RBF were used from these mathematical functions. Eq. (5) is used for the normalization process and Eqs. (6)–(8) are used for calculation of polynomial, RBF and linear kernel functions, respectively.

$$y = \frac{x_i - x_{\min}}{x_{\max} - x_{\min}} \tag{5}$$

where y is the normalized value of x_i, $x_{\max}$ is the maximum value of x_i, and $x_{\min}$ is the minimum value of x_i.

$$\text{Polynomial kernel: } k\left(x_i, x_j\right) = \left(x_i x_j + 1\right)^d \tag{6}$$

$$\text{RBF kernel: } k\left(x_i, x_j\right) = \exp\left(-\gamma \left\| x_i - x_j \right\|^2\right)$$

$$\gamma = \frac{1}{2\sigma^2} \quad \text{for} \quad \gamma > 0 \tag{7}$$

$$\text{Linear kernel: } k\left(x_i, x_j\right) = x_i^T x_j \tag{8}$$

2.5. Isotherm, kinetic, and thermodynamic studies of Malachite green adsorption onto kaolinite

2.5.1. Adsorption isotherm studies

Many isotherm models are used to identify the interaction between adsorbate and adsorbent molecules. Dubinin–Radushkevich (D-R), Freundlich, and Langmuir isotherms were chosen to explain the interaction of MG molecules and the kaolinite surface in this study. These three models were applied to the experimental results which were obtained at three different temperatures. There are assumptions about adsorption occurrence on a homogenous surface and no interaction between adsorbates in the plane of the surface in the Langmuir isotherm model, with equation given by Eq. (9):

$$q_e = \frac{\left(q_m K_L C_e\right)}{\left(1 + K_L C_e\right)} \tag{9}$$

where q_m denotes the maximum capacity of adsorption (mg g^{-1}), C_e represents equilibrium concentration of solution (mg L^{-1}), and K_L is a Langmuir constant associated with affinity of the binding sites and energy of adsorption (L g^{-1}). A linear form of Eq. (9) is obtained when $1/C_e$ vs. $1/q_e$ is plotted, and q_m and K_L can be determined from the slope and intercept. The Freundlich isotherm is an empirical model based on adsorption occurring on a heterogeneous surface and its equation is given in Eq. (10):

$$q_e = K_F C_e^{1/n} \tag{10}$$

where K_F is the Freundlich constant (L g^{-1}), and n is an empirical coefficient. A straight line is obtained for the plot of the natural logarithm of q_e vs. C_e. The slope and intercept of the line gives the n and K_F values, respectively. The D-R isotherm model is used to explain heterogeneous adsorption with Gaussian energy distribution. This model is generally applied to distinguish the physical and chemical adsorption of ions by their average free energy (E), which is determined per molecule of adsorbate for this relationship. This isotherm equation is given by Eq. (11):

$$\ln\left(q_e\right) = \ln\left(q_m\right) - K_D \times \varepsilon^2 \tag{11}$$

where q_m is the saturation capacity (mg g^{-1}), K_D is a D-R constant (mol² kJ^{-2}) and ε is the D-R isotherm constant which is also known as the Polanyi potential. The slope and intercept of $\ln(q_e)$ vs. ε^2 plot give the K_D and $\ln(q_m)$ values, respectively. The D-R isotherm constant, ε, is expressed with Eq. (12):

$$\varepsilon = RT\ln\left[1+\left(\frac{1}{C_e}\right)\right] \tag{12}$$

where R is the gas constant (8.314×10^{-3} kJ mol^{-1} K^{-1}) and T is temperature (K). The mean free energy, E (kJ mol^{-1}), of the sorption per molecule of adsorbate is obtained from K_D, and the equation is given by Eq. (13):

$$E = \frac{1}{\sqrt{2K_D}} \tag{13}$$

2.5.2. Adsorption kinetic studies

Kinetic models were applied to check the experimental results of MG adsorption onto kaolinite. The adsorption kinetics are important to choose the best test circumstances for the adsorption process with the batch technique. The kinetic parameters for estimation of adsorption rate provide vital knowledge for designing and modelling adsorption processes. Kinetic models are widely used in adsorption operations to investigate the mechanisms that control the removal process, such as the adsorption surface, chemical reaction and/or diffusion mechanisms. In this study, MG adsorption kinetics were calculated using pseudo-first-order, pseudo-second-order and intraparticle diffusion kinetic models. The best fit model was chosen depending on the correlation coefficient (R^2) values. These models were investigated according to experimental data at various temperatures and initial TB concentrations.

Lagergren's equation, which is called the pseudo-first-order kinetic model, separates the equation depending on the concentration of solution and solid adsorption capacity. The pseudo-first-order linear model is given by Eq. (14):

$$\ln\left(q_e - q_t\right) = \ln q_e - k_1 t \tag{14}$$

where k_1 (min^{-1}) is the rate constant for the pseudo-first-order model. To obtain the constants for this model, plots of $\ln(q_e - q_t)$ against t are drawn.

The pseudo-second-order kinetic model explains chemical bond formation between adsorbent and adsorbate molecules based on adsorption capacity. The linear form of the pseudo-second-order model based on adsorption capacity is given with Eq. (15):

$$\frac{t}{q_t} = \frac{1}{\left(k_2 q_e^2\right)} + \frac{t}{q_e} \tag{15}$$

where k_2 represents rate of adsorption (g mg^{-1} min^{-1}) and the values of k_2 and q_e are identified from intercept and slope of the plot of t/q_t vs. t, respectively.

Adsorption of dyes is more gradual when intraparticle diffusion is the rate controlling step. The intraparticle diffusion model assumes that the chemical or physical bond formed between solute and solid in interspatial sites on the solid control the overall speed of adsorption. The possibility of intraparticle diffusion as the rate-limiting step was tested using the intraparticle diffusion model, which can be represented by Eq. (16):

$$q_t = k_{\text{ipd}} t^{0.5} + C \tag{16}$$

where k_{ipd} (mg g^{-1} min$^{-0.5}$) is the intraparticle diffusion rate constant and C is boundary thickness, which are determined from the plot of q_t against $t^{0.5}$ at different MG concentrations.

2.5.3. Adsorption thermodynamic studies

Thermodynamic investigation is required to determine the significance of adsorption processes. The variations in Gibbs free energy $\Delta G°$ (kJ mol^{-1}), enthalpy $\Delta H°$ (kJ mol^{-1}), and entropy $\Delta S°$ (kJ mol^{-1} K^{-1}) are significant to detect heat alterations during the adsorption process. The thermodynamic parameters of MG adsorption onto kaolinite were calculated by the equations given below:

$$\Delta G° = -RT\ln K_d \tag{17}$$

$$\Delta G° = \Delta H° - T\Delta S° \tag{18}$$

$$\ln K_d = \frac{\Delta S°}{R} - \frac{\Delta H°}{RT} \tag{19}$$

where K_d is the equilibrium constant (q_e/C_e; L g^{-1}), R is the gas constant and T is temperature (K). $\Delta H°$ and $\Delta S°$ parameters are calculated from slope and intercept of the plot of $\ln K_d$ vs. $1/T$.

3. Results and discussion

3.1. Effects of contact time, temperature and initial dye concentrations for MG adsorption on kaolinite

Contact time and initial concentration effects of MG adsorption on kaolinite are shown in Fig. 5a–c for 298, 308 and 318 K, respectively. These figures show the removal percentage curves which indicate that MG adsorption speed is very high for the first period and remains constant after 100 min indicating equilibrium. The migration of MG molecules in the solution can easily access the vacant sites on the adsorbent in the initial period. However, in the next period, adsorption decreases due to the slower diffusion of dissolved molecules through the adsorbent pores. The rapid removal of dye facilitates the use of decreased adsorbent volumes and thus ensures efficiency and lower costs of the operation. As the initial dye concentration increased from 10 to 60 mg L^{-1}, the removal percentage of MG on kaolinite increased from 68.71% to 79.61% for 298 K, 72.26% to 82.58% for 308 K and 78.75% to 85.91% for 318 K, respectively. After batch experiments, 68.71%, 72.26% and 78.75% removal percentages for MG were achieved with kaolinite for 10 mg L^{-1} initial dye concentration at 298, 308 and 318 K, respectively. Removal percentages of 74.16%, 76.49% and 82.44% for MG were obtained with kaolinite for 40 mg L^{-1} initial dye concentration at 298, 308 and 318 K, respectively. Comparatively, 79.61%, 82.58% and 85.91% removal percentages were obtained for 60 mg L^{-1} initial dye concentration at 298, 308 and 318 K,

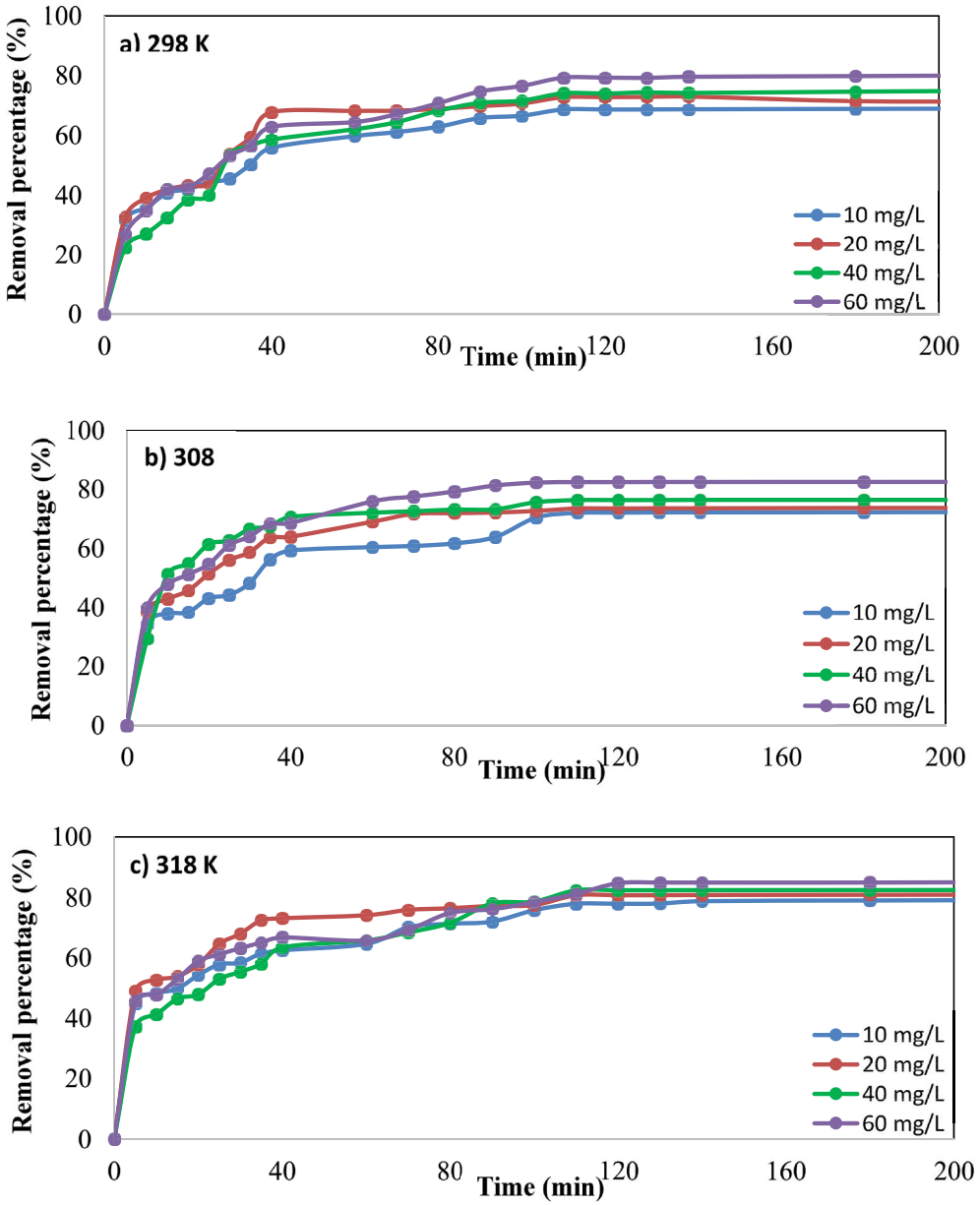

Fig. 5. Removal percentage for MG adsorption on kaolinite at three temperatures: (a) 298 K, (b) 308 K and (c) 318 K.

respectively. According to the results, kaolinite has higher removal capacity for adsorption of MG. The experimental data indicate that the initial dye concentration and temperature play important roles in dye adsorption capacity and provide interaction between the adsorbent and the dye molecules. Increasing the initial dye concentration results in an increase in the adsorption capacity because it supplies a driving force to overcome all mass transfer resistances of dye between the aqueous and solid phase. However, the adsorbent has a limited number of active sites, which become saturated at a certain concentration. This indicates that the adsorption capacity will increase with the increase of initial dye concentration mainly due to the elevation of mass transfer from the concentration gradient.

3.2. Results of machine learning methods for removal of MG adsorption on kaolinite

MATLAB and Python programs were used for the machine learning applications developed for this study. These applications were run on a computer with 8 GB RAM and I5 processor. The data set used for the study consists of three attributes and eighty samples. Initial dye concentration, contact time and temperature values, which are the three attributes, were used in applications as the input data and removal percentage value was the target value. Input and output data were normalized in the range of 0–1 for attributes using Eq. (5). In this study, mean squared error (MSE), root mean square error (RMSE) values and

coefficient of determination (R^2) were used to evaluate the model results [37]. MSE, RMSE and R^2 values showed the efficiency of these machine learning methods and they were calculated with Eqs. (20)–(22), respectively.

$$\mathrm{MSE} = \frac{1}{N}\sum_{i=1}^{N}\left(\left|y_{\mathrm{prd},i} - y_{\mathrm{exp},i}\right|\right)^2 \tag{20}$$

$$\mathrm{RMSE} = \sqrt{\frac{\sum_{i=1}^{N}\left(y_{\mathrm{prd},i} - y_{\mathrm{exp},i}\right)^2}{N}} \tag{21}$$

$$R^2 = 1 - \frac{\sum_{i=1}^{N}\left(y_{\mathrm{prd},i} - y_{\mathrm{exp},i}\right)^2}{\sum_{i=1}^{N}\left(y_{\mathrm{prd},i} - y_m\right)^2} \tag{22}$$

where $y_{\mathrm{prd},i}$ is the ith predicted value, $y_{\mathrm{exp},i}$ is the ith observed value, y_m is the mean value of $y_{\mathrm{exp},i}$, and N is the number of observations. R^2 shows the fit of the predicted output variable estimation curve to the experimental data output variable curve. Higher R^2 with lower MSE and RMSE values indicate a model with better output prediction and better performance.

The ANN parameters used in this study were train ratio 0.7, validation ratio 0.15, test ratio 0.15, and the Levenberg Marquardt transfer function algorithm was used for error minimization. ANN results for Malachite green adsorption on kaolinite are given in Table 1. The results of ANN were obtained by increasing the number of hidden layers in the range of 1–10. The average values of R^2 for the ANN model were observed to be 0.9681, 0.9728 and 0.9616 for 298, 308 and 318 K, respectively. When the average R^2 values of the ANN model are compared, the average R^2 values obtained at 308 K are higher than for the temperatures of 298 and 318 K. In general, R^2 values increased and MSE, RMSE values decreased with the increase in the temperature. The lowest MSE and RMSE values for the ANN model were determined as 0.00148 and 0.03556 for 308 K, respectively. The low MSE and RMSE values showed that the training network did not have any over-fitting problem. The high correlation and predictive accuracy of the ANN model was attributed to its well-known ability to approximate the non-linearity of the system [38]. The ANN model showed good performance with highest R^2 (0.9658) and the lowest MSE (0.0017) values compared to the multiple linear regression model for Malachite green adsorption onto copper nanowires loaded on activated carbon [39].

The RBFNN parameters used in this study were spread of radial basis functions 0.2, mean squared error goal 0, and transfer function radbas. The average R^2 values obtained by the RBFNN were 0.98 for the three temperatures. These values were obtained by increasing the number of hidden layers and R^2 values of 0.99 were obtained after the 20th hidden layer for the three temperatures. The lowest RMSE values were determined as 0.011 for 298 and 308 K and the lowest MSE values were obtained as 0.0001 for all three temperatures. Detailed RBFNN results are given in Table 2.

SVR model results for Malachite green adsorption on kaolinite obtained for linear, polynomial and RBF kernel functions are given in Table 3. The GridSearchCV method was used to determine the appropriate parameters in the formation of SVR and RF models. This method allows parameters to be found that give the best results by using the values of the parameters one by one at specified intervals. Using this method, the parameter values were found for 298 K as follows; linear kernel: C = 1.0, ε = 0.05, polynomial kernel: C = 1,000, ε = 0.001, and RBF kernel: C = 1,000, ε = 0.005. The linear kernel gave the worst R^2 results with the value of 0.74 for 308 and 318 K temperatures. The polynomial kernel achieved better R^2 values than other temperatures for 298 K with the value of 0.92. Similar to the polynomial kernel, better

Table 1
ANN results for MG adsorption on the kaolinite

Number of neurons	298 K			308 K			318 K		
	R^2	RMSE	MSE	R^2	RMSE	MSE	R^2	RMSE	MSE
1	0.9357	0.0631	0.0043	0.8984	0.0745	0.0055	0.8675	0.0834	0.0071
2	0.9426	0.0595	0.0035	0.9528	0.0508	0.0026	0.9149	0.0669	0.0045
3	0.9733	0.0406	0.0017	0.9796	0.0333	0.0011	0.9621	0.0446	0.0023
4	0.9709	0.0424	0.0018	0.9778	0.0348	0.0012	0.9688	0.0405	0.0016
5	0.9723	0.0413	0.0017	0.9846	0.0291	0.0008	0.9867	0.0264	0.0007
6	0.9718	0.0417	0.0017	0.9854	0.0283	0.0008	0.9725	0.0381	0.0014
7	0.9759	0.0386	0.0015	0.9852	0.0284	0.0008	0.9832	0.0297	0.0009
8	0.9776	0.0372	0.0014	0.9899	0.0235	0.0006	0.9902	0.0227	0.0005
9	0.9718	0.0417	0.0017	0.9854	0.0282	0.0008	0.9846	0.0284	0.0008
10	0.9892	0.0258	0.0007	0.9888	0.0248	0.0006	0.9855	0.0276	0.0008
Avg.	0.96811	0.04318	0.00197	0.97279	0.03556	0.00148	0.9616	0.04082	0.00202
Std.	0.01541	0.01016	0.00095	0.02678	0.01488	0.00145	0.03771	0.01872	0.00199
Min.	0.9357	0.0258	0.0007	0.8984	0.0235	0.0006	0.8675	0.0227	0.0005
Max.	0.9892	0.063	0.004	0.9899	0.0745	0.0055	0.9902	0.0834	0.007

Table 2
RBFNN results for MG adsorption on the kaolinite

Number of neurons	298 K			308 K			318 K		
	R^2	RMSE	MSE	R^2	RMSE	MSE	R^2	RMSE	MSE
10	0.9622	0.0483	0.0023	0.9426	0.0563	0.0031	0.9693	0.0828	0.0069
20	0.9907	0.024	0.0006	0.9884	0.0252	0.0006	0.9735	0.0373	0.0014
50	0.9967	0.0143	0.0002	0.9963	0.0142	0.0002	0.9966	0.0133	0.0002
80	0.9981	0.011	0.0001	0.9977	0.0112	0.0001	0.9989	0.0078	0.0001
Avg.	0.986925	0.0244	0.0008	0.98125	0.02665	0.001	0.984575	0.0353	0.00215
Std.	0.014543	0.014603	0.000886	0.022595	0.017728	0.001227	0.0530585	0.029583	0.002789
Min.	0.9622	0.0113	0.0001	0.9426	0.0112	0.0001	0.8693	0.0078	0.0001
Max.	0.9981	0.0483	0.0023	0.9977	0.0563	0.0031	0.9989	0.0828	0.0069

Table 3
SVR results for MG adsorption on the kaolinite

Kernel	298 K			308 K			318 K		
	MSE	RMSE	R^2	MSE	RMSE	R^2	MSE	RMSE	R^2
Linear	0.014771	0.12155	0.76144	0.014191	0.119121	0.74113	0.013447	0.115959	0.74594
Polynomial	0.003429	0.05855	0.92825	0.005135	0.071656	0.85284	0.005323	0.072956	0.87151
RBF	0.003371	0.05806	0.92771	0.004529	0.067298	0.89824	0.005154	0.071794	0.90265

R^2 values were obtained with RBF kernel at 298 K. The lowest MSE and RMSE values were determined as 0.003371 and 0.05806 for 298 K, respectively. MSE and RMSE values were close to each other for polynomial and RBF kernels at 298 K.

The obtained RF model results for Malachite green adsorption on kaolinite are given in Table 4. The Grid SearchCV method was used for the selection of suitable parameters for this model. The max_depth value obtained by this method was 6. While obtaining results, the n_estimator parameter increased by 10 and reached up to 200. This parameter represents the number of trees in the random forest. The average and maximum R^2 values were obtained as 0.97 and 0.98 for the three temperatures, respectively. The lowest MSE and RMSE values were determined as 0.00112 and 0.0334 for 318 K, respectively. The obtained graphical scores as a result of these experiments are given in Fig. 6. It is possible to see the effect of estimators for the three temperature values. The RF model showed the best performance with the highest R^2 (0.994) and the lowest RMSE (1.92) values compared to Bayesian multiple linear regression and multiple linear regression models for 2,4-dichlorophenoxy acetic acid adsorption by rice husk biochar from synthetic wastewater [40]. Similarly, the highest R^2 (0.9895) and lowest MSE (0.0006) values were obtained with the RF model compared to multiple linear regression model for bromophenol blue adsorption by activated carbon which was derived from the *Astragalus bisulcatus* tree [41].

It is possible to see the results of all models in Table 5. If we examine this table, the best results were obtained from ANN among the models used in our study. If a model comparison is made on the basis of temperature, the best R^2 value was obtained at 308 K from ANN with 0.9728. RBFNN and RFR model results were close to each other. At 308 K, the RF model achieved the highest value with 0.97895 R^2 value. ANN and RBFNN models were also close to this value. Here, like the 298 K temperature, the SVR model achieved worse results compared to the other models. Finally, when the temperature of 318 K is examined, the ANN model obtained a better result with R^2 value of 0.9862 compared to the other models. It is possible to see that RBFNN and then RF get better results than SVR compared to the other models, respectively. The results

Table 4
RF model results for MG adsorption on kaolinite

	298 K			308 K			318 K		
	MSE	RMSE	R^2	MSE	RMSE	R^2	MSE	RMSE	R^2
Avg.	0.00186	0.04298	0.9761	0.00164	0.04011	0.97844	0.00168	0.0409	0.9771
Min.	0.00151	0.03893	0.9638	0.00114	0.03379	0.95317	0.00112	0.0334	0.9708
Max.	0.00282	0.05315	0.9805	0.00356	0.05973	0.98501	0.00214	0.0463	0.9847

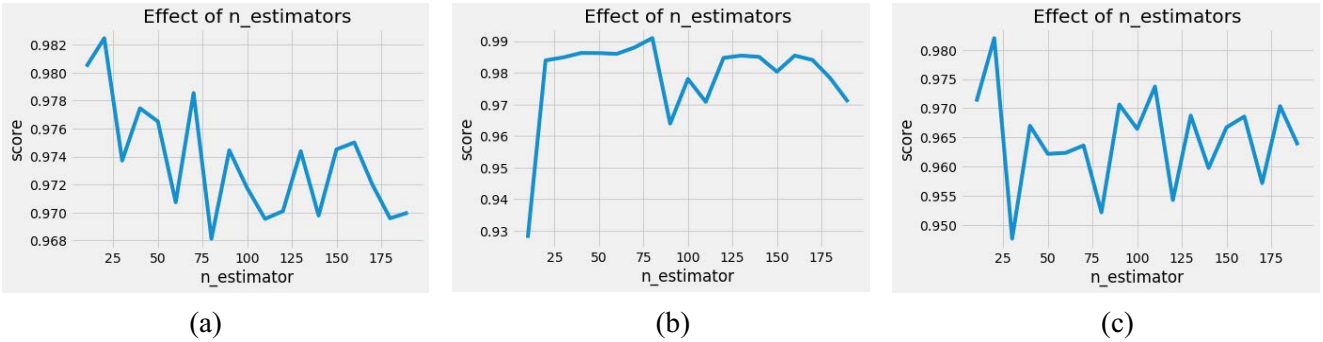

(a) (b) (c)

Fig. 6. Effects of RF model estimators for different temperatures: (a) 298 K, (b) 308 K and (c) 318 K.

obtained from applied machine learning methods are compared in Fig. 7. The highest R^2 values and the lowest MSE and RMSE values were determined with ANN model for the three temperatures. R^2 values of RBF and RF models were close to the ANN model for the three temperatures. RF and ANN models exhibited similar performances according to their R^2 values of 0.9739 and 0.9734, as well as their MSE values of 0.0012 and 0.0016 for methylene blue adsorption on residual agricultural biomass (orange bagasse), respectively [34]. The lowest R^2 values were obtained with the SVR model with linear kernel and the highest MSE and RMSE values were determined with RF model for the three temperatures. ANN and RF models were used for the adsorption of Malachite green with jackfruit seed and high R^2 values of 0.966 and 0.981 and low RMSE values of 0.048 and 0.038 were obtained, respectively [42].

3.3. Isotherm results of Malachite green adsorption onto kaolinite

D-R, Freundlich, and Langmuir isotherm models were chosen to explain the interaction of adsorbate molecules and adsorbent surface in this study. All models were applied for the description of the experimental data obtained at three temperatures. The coefficients of these isotherm models determined for adsorption of MG onto kaolinite are presented in Table 6. R^2 values of the Langmuir model were higher than the Freundlich and D-R model values. With respect to the coefficients, the Langmuir model

Table 5
Numerical results of applied models for MG adsorption on kaolinite

Method	298 K			308 K			318 K		
	MSE	RMSE	R^2	MSE	RMSE	R^2	MSE	RMSE	R^2
ANN	0.000808	0.02263	0.986917	0.001181	0.03013	0.978357	0.000721	0.019017	0.986275
RBFNN	0.0193933	0.028275	0.97855	0.010281	0.02695	0.974575	0.02102	0.02775	0.97135
RF	0.036799	0.191262	0.973634	0.034255	0.178596	0.978958	0.057994	0.239267	0.964613
SVR_L	0.014771	0.12155	0.76144	0.014191	0.119121	0.74113	0.013447	0.115959	0.74594
SVR_P	0.003429	0.05855	0.92825	0.005135	0.071656	0.85284	0.005323	0.072956	0.87151
SVR_RBF	0.003371	0.05806	0.92771	0.004529	0.067298	0.89824	0.005154	0.071794	0.90261

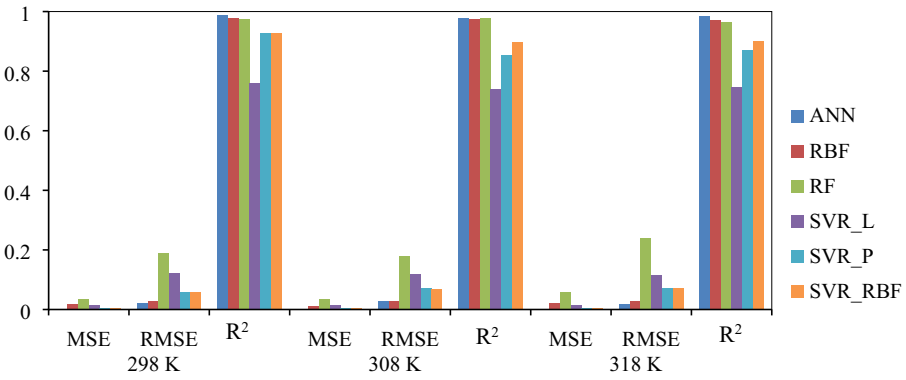

Fig. 7. Graphical results of applied machine learning models for MG adsorption on kaolinite.

Table 6
Isotherm model constants for MG adsorption onto kaolinite

Isotherm/Temperature	298 K	308 K	318 K
Langmuir			
K_L (L g^{-1})	0.033	0.038	0.046
q_m (mg g^{-1})	50.665	54.737	57.945
R^2	1.000	0.994	0.998
Freundlich			
K_F (mg g^{-1})(L mg^{-1})$^{1/n}$	1.219	1.850	3.019
$1/n$	0.852	0.864	0.873
R^2	0.990	0.970	0.995
Dubinin–Radushkevich			
$K_{D\text{-}R}$	0.002	0.003	0.005
E (kJ mol^{-1})	10.541	13.131	16.667
R^2	0.861	0.827	0.888

fit better than the Freundlich and D-R isotherm models and this indicates that the adsorption of MG on kaolinite takes place as monolayer adsorption on a surface that is homogenous in terms of adsorption affinity [43]. The K_F and n values increase as temperature increases, and also indicate that adsorption is more favorable at higher temperatures. Monolayer adsorption capacity (q_m) values were determined as 50.67, 54.74 and 57.95 mg g^{-1} for 298, 308 and 318 K, respectively. The adsorption intensity (K_L) is the Langmuir constant, which expresses the affinity of the binding sites in relation to energy. The K_L values were obtained as 0.033, 0.038 and 0.046 L mg^{-1} for 298, 308 and 318 K, respectively. The K_L values increased with the increase in temperature, which accounts for the endothermic nature of the adsorption process. The separation factor (R_L) is used as a dimensionless constant in equilibrium concentration studies. If R_L is greater than 1, it is concluded that adsorption is unsuitable and if the calculated R_L value is between 0 and 1, adsorption is favorable. The R_L values for the adsorption of MG onto kaolinite are in the range of 0.675–0.906, indicating that the adsorption is a favorable process and that the adsorption is nearly irreversible at initial MG concentrations. The n values were determined from the Freundlich isotherm and $1/n$ values show the adsorption intensity was higher than 1.0, which indicates good adsorption by kaolinite clay. The K_F values were obtained as 1.219, 1.850 and 3.019 L mg^{-1} for 298, 308 and 318 K, respectively. The increase in Freundlich constants with the increase of temperature confirmed that adsorption was favorable at high temperatures and the process was endothermic in nature. The D-R model is generally applied to distinguish the physical and chemical adsorption of ions by their average free energy (E) which is determined per molecule of adsorbate for this relationship. The calculated energy values from the D-R equation were 10.541, 13.131 and 16.667 kJ mol^{-1} for MG adsorption onto kaolinite at 298, 308 and 318 K, respectively. E values were higher than 8 kJ mol^{-1} for all studied temperatures indicating that chemical adsorption takes place.

Various studies in the literature investigated the usage of different adsorbents and biosorbents for MG adsorption. Comparison of the monolayer adsorption capacity values of MG by various adsorbents are given in Table 7. When the results of case studies and those of the present study are compared, kaolinite has a relatively large adsorption capacity for MG. This suggests that MG could be easily adsorbed on kaolinite and it can be used as an abundant, inexpensive and effective adsorbent for MG removal from aqueous solutions.

3.4. Kinetic results for Malachite green adsorption onto kaolinite

Kinetic parameters in the pseudo-first-order, pseudo-second-order and intraparticle diffusion models for MG adsorption onto kaolinite are given in Table 8. The correlation coefficient R^2 values of the pseudo-first-order and intraparticle diffusion kinetic models are lower than the pseudo-second-order kinetic model; thus, these models are not rate-limiting steps. The R^2 (>0.990) for the pseudo-second-order kinetic model was close to 1.0 and indicates that the highest R^2 coefficients with calculated q_e values for the process best fits the pseudo-second-order model. The pseudo-second-order kinetic results show that the theoretical q_e and the experimental q_e values are relatively close compared to the other models. The adsorption process of MG on kaolinite may be dominated by chemical adsorption. According to the kinetic results, it is obvious that the q_e values determined using pseudo-first-order, pseudo-second-order and intraparticle diffusion models increased with increasing temperature and initial dye concentration (Table 8). Kinetic results show that MG adsorption on kaolinite abides by the pseudo-second-order model and suggests that the rate-limiting step is explained by electron exchange between the kaolinite and MG molecules. Kinetic data for adsorption is better represented by a pseudo-second-order model for most dye removal processes [56,57].

Table 7
Comparison of the MG adsorption capacity of various adsorbents

Adsorbent	Adsorption capacity (mg g^{-1})	Reference
Ni:FeO(OH)-NWs-AC	29.81	[44]
Potato peel	32.39	[45]
Luffa aegyptiaca peel	70.21	[46]
Annona squamosa seed	25.91	[47]
Wood apple shell	34.56	[48]
Seed hull	8.40	[49]
Rice husk	24.92	[50]
Copperpod fruit shell	62.50	[51]
Sea shell powder	42.33	[52]
Diatomite	23.64	[53]
Rattan sawdust	62.71	[54]
Coal fly ash/$CoFe_2O_4$	89.32	[55]
Kaolinite	57.95	This study

Table 8
Kinetic model parameters for MG adsorption onto kaolinite

Kinetic model	Temp. (K)	Kinetic constant	10 (mg L^{-1})	20 (mg L^{-1})	40 (mg L^{-1})	60 (mg L^{-1})
	298	q_{exp} (mg g^{-1})	6.568	13.584	28.554	45.774
	308	q_{exp} (mg g^{-1})	7.167	14.328	29.709	48.123
	318	q_{exp} (mg g^{-1})	7.756	15.863	31.714	49.554
	298	k_1 (min^{-1})	0.037	0.030	0.032	0.033
		q_e (mg g^{-1})	5.924	6.653	25.868	43.423
		R^2	0.947	0.873	0.966	0.956
	308	k_1 (min^{-1})	0.041	0.043	0.056	0.053
Pseudo-first-order		q_e (mg g^{-1})	7.776	10.044	28.191	49.452
		R^2	0.896	0.983	0.930	0.954
	318	k_1 (min^{-1})	0.032	0.041	0.048	0.036
		q_e (mg g^{-1})	5.778	10.591	44.124	44.970
		R^2	0.952	0.923	0.883	0.854
	298	k_2 (min^{-1})	0.010	0.008	0.002	0.001
		q_e (mg g^{-1})	6.99	13.49	30.03	48.35
		R^2	0.996	0.995	0.992	0.993
	308	k_2 (min^{-1})	0.012	0.010	0.006	0.003
Pseudo-second-order		q_e (mg g^{-1})	7.63	14.93	32.30	50.00
		R^2	0.993	0.999	0.999	0.998
	318	k_2 (min^{-1})	0.013	0.010	0.006	0.002
		q_e (mg g^{-1})	8.06	16.39	34.48	52.63
		R^2	0.996	0.999	0.993	0.993
	298	k_{int} (mg g^{-1} $min^{-0.5}$)	0.554	1.235	4.046	2.283
		C (mg g^{-1})	1.291	2.737	5.916	12.349
		R^2	0.920	0.887	0.954	0.953
	308	k_{int} (mg g^{-1} $min^{-0.5}$)	0.571	1.218	4.130	2.452
Intraparticle diffusion		C (mg g^{-1})	1.503	3.757	11.585	18.875
		R^2	0.885	0.860	0.887	0.770
	318	k_{int} (mg g^{-1} $min^{-0.5}$)	0.567	1.199	2.563	3.488
		C (mg g^{-1})	2.26	5.28	16.19	24.18
		R^2	0.811	0.760	0.917	0.796

3.5. Thermodynamic results for Malachite green adsorption onto kaolinite

Thermodynamic parameters for MG adsorption onto kaolinite were calculated using Eqs. (17)–(19) and the Gibbs free energy ($\Delta G°$), enthalpy ($\Delta H°$), and entropy ($\Delta S°$) values are given in Table 9. The values obtained for $\Delta G°$ and $\Delta H°$ can help in describing the mechanism of the adsorption process. $\Delta G°$ values for MG adsorption onto kaolinite were determined as –2.919, –3.531, and 4.143 kJ mol^{-1} for 298 K, 308 K and 318 K, respectively. $\Delta H°$ and $\Delta S°$ values for MG removal with kaolinite were calculated as 15.318 kJ mol^{-1} and 61.201 J mol^{-1} K^{-1}, respectively. The $\Delta G°$ values, which varied between 0 and –30 kJ mol^{-1}, show the feasibility of this removal process and spontaneous nature of MG adsorption on kaolinite (Table 9). The absolute values of $\Delta G°$ increase as the temperature increases showing that this separation process is better at high temperatures. Accordingly, the increase in dye removal with increasing temperatures is due to chemical bonds, electrostatic interactions and Van der Waals forces between MG and kaolinite. The positive $\Delta H°$ value shows that the removal process is endothermic and the positive $\Delta S°$ value establishes enhanced randomness at the kaolinite–dye interface and the affinity of kaolinite for MG [58].

4. Conclusions

The presence of synthetic dyes in water sources causes serious issues due to poor water quality, toxicity to the environment and human carcinogenic effects. Adsorption has progressively become an economical and feasible method for dye wastewater decontamination. Clay minerals are an interesting alternative for removing colorants from colored aqueous solutions because they are inexpensive, easy to extract and handle, and non-toxic. In this study, machine learning methods were used to estimate the adsorption percentage of Malachite green dye on kaolinite. When the average results were analyzed, ANN provided the most efficient results for estimating removal percentage. The successful performances of other methods are given comparatively. Metric values of R^2, MSE and RMSE were used for model evaluations. In comparative results, ANN, RBFNN, and RF

Table 9
Thermodynamic parameters for Malachite green adsorption onto kaolinite

Temp. (K)	$\Delta G°$ (kJ mol^{-1})	$\Delta H°$ (kJ mol^{-1})	$\Delta S°$ (J mol^{-1} K^{-1})	R^2
298	–2.919			
308	–3.531	15.318	61.201	0.992
318	–4.143			

models were shown to give good results for different temperatures. In order to achieve the purpose of this study, it is foreseen that these methods can be used in estimation studies for chemical processes. It is thought that workloads will decrease if researchers working in this field gain ideas from this study and use these models in their research. The experimental data of removal percentages showed that the initial dye concentration and process temperatures plays a crucial role in dye adsorption capacity and provides a driving force in the interaction between the adsorbent and dye. The adsorption equilibrium data were found to best fit the Langmuir isotherm at all studied temperatures, indicating adsorption on a homogenous surface. The adsorption data showed the best agreement with the pseudo-second-order kinetic model for different initial dye concentrations. The rate constant increased with the increase in temperature indicating the endothermic nature of adsorption. Thermodynamic analysis of the obtained data suggests that the adsorption process is spontaneous and endothermic in nature.

Information about paper

This study did not receive any specific grant from funding agencies in the public, commercial, or non-profit sectors. The authors declare no conflict of interest. No additional information is available for this paper.

References

[1] A. Dehbi, Y. Dehmani, H. Omari, A. Lammini, K. Elazhari, A. Abdallaoui, Hematite iron oxide nanoparticles (α-Fe_2O_3): synthesis and modelling adsorption of Malachite green, J. Environ. Manage., 8 (2020) 103394, doi: 10.1016/j.jece.2019.103394.
[2] A. Verma, S. Thakur, G. Mamba, Prateek, R.K. Gupta, P. Thakur, V.K. Thakur, Graphite modified sodium alginate hydrogel composite for efficient removal of Malachite green dye, Int. J. Biol. Macromol., 148 (2020) 1130–1139.
[3] A. Yildirim, Y. Bulut, Adsorption behaviors of Malachite green by using crosslinked chitosan/polyacrylic acid/bentonite composites with different ratios, Environ. Technol. Innovation, 17 (2020) 100560, doi: 10.1016/j.eti.2019.100560.
[4] T.P. Krishna Murthy, B.S. Gowrishankar, M.N. Chandra Prabha, M. Kruthi, R. Hari Krishna, Studies on batch adsorptive removal of Malachite green from synthetic wastewater using acid treated coffee husk: equilibrium, kinetics and thermodynamic studies, Microchem. J., 146 (2019) 192–201.
[5] E.B. Azimi, A. Badiei, J.B. Ghasemi, Efficient removal of Malachite green from wastewater by using boron-doped mesoporous carbon nitride, Appl. Surf. Sci., 469 (2019) 236–245.
[6] E. Altintig, M. Onaran, A. Sarı, H. Altundag, M. Tuzen, Preparation, characterization and evaluation of bio-based magnetic activated carbon for effective adsorption of Malachite green from aqueous solution, Mater. Chem. Phys., 220 (2018) 313–321.
[7] V. Katheresan, J. Kansedo, S.Y. Lau, Efficiency of various recent wastewater dye removal methods: a review, J. Environ. Chem. Eng., 6 (2018) 4676–4697.
[8] F. Naseeruteen, N.S. Abdul Hamid, F.B. Mohd Suah, W.S. Wan Ngah, F.S. Mehamod, Adsorption of Malachite green from aqueous solution by using novel chitosan ionic liquid beads, Int. J. Biol. Macromol., 107 (2018) 1270–1277.
[9] F. Guo, X. Jiang, X. Li, X. Jia, S. Liang, L. Qian, Synthesis of MgO/Fe_3O_4 nanoparticles embedded activated carbon from biomass for high-efficient adsorption of Malachite green, Mater. Chem. Phys., 240 (2020) 122240, doi: 10.1016/j.matchemphys.2019.122240.
[10] M. Mobarak, E.A. Mohamed, A.Q. Selim, M.F. Eissa, M.K. Seliem, Experimental results and theoretical statistical modeling of Malachite green adsorption onto MCM–41 silica/rice husk composite modified by beta radiation, J. Mol. Liq., 273 (2019) 68–82.
[11] D. Robati, M. Rajabi, O. Moradi, F. Najafi, I. Tyagi, S. Agarwal, V.K. Gupta, Kinetics and thermodynamics of Malachite green dye adsorption from aqueous solutions on graphene oxide and reduced graphene oxide, J. Mol. Liq., 214 (2016) 259–263.
[12] K.G. Pavithra, P.S. Kumar, V. Jaikumar, P.S. Rajan, Removal of colorants from wastewater: a review on sources and treatment strategies, J. Ind. Eng. Chem., 75 (2019) 1–19.
[13] R. Bagheri, M. Ghaedi, A. Asfaram, E.A. Dil, H. Javadian, RSM-CCD design of Malachite green adsorption onto activated carbon with multimodal pore size distribution prepared from *Amygdalus scoparia*: kinetic and isotherm studies, Polyhedron, 171 (2019) 464–472.
[14] F. Jiang, D.M. Dinh, Y.-L. Hsieh, Adsorption and desorption of cationic Malachite green dye on cellulose nanofibril aerogels, Carbohydr. Polym., 173 (2017) 286–294.
[15] Y. Zhou, J. Lu, Y. Zhou, Y. Liu, Recent advances for dyes removal using novel adsorbents: a review, Environ. Pollut., 252 (2019) 352–365.
[16] N.B. Singh, G. Nagpal, S. Agrawal, Rachna, Water purification by using adsorbents: a review, Environ. Technol. Innovation, 11 (2018) 187–240.
[17] S. De Gisi, G. Lofrano, M. Grassi, M. Notarnicola, Characteristics and adsorption capacities of low-cost sorbents for wastewater treatment: a review, Sustainable Mater. Technol., 9 (2016) 10–40.
[18] T. Ngulube, J.R. Gumbo, V. Masindi, A. Maity, An update on synthetic dyes adsorption onto clay based minerals: a state-of-art review, J. Environ. Manage., 191 (2017) 35–57.
[19] A. Kausar, M. Iqbal, A. Javed, K. Aftab, Z.-H. Nazli, H.N. Bhatti, S. Nouren, Dyes adsorption using clay and modified clay: a review, J. Mol. Liq., 256 (2018) 395–407.
[20] M. Rajabi, K. Mahanpoor, O. Moradi, Preparation of PMMA/GO and PMMA/GO-Fe_3O_4 nanocomposites for Malachite green dye adsorption: kinetic and thermodynamic studies, Composites, Part B, 167 (2019) 544–555.
[21] S. Agarwal, I. Tyagi, V.K. Gupta, S. Mashhadi, M. Ghasemi, Kinetics and thermodynamics of Malachite green dye removal from aqueous phase using iron nanoparticles loaded on ash, J. Mol. Liq., 223 (2016) 1340–1347.
[22] M.A. Ahmad, R. Alrozi, Removal of Malachite green dye from aqueous solution using rambutan peel-based activated carbon: equilibrium, kinetic and thermodynamic studies, Chem. Eng. J., 171 (2011) 510–516.

[23] N. Parveen, S. Zaidi, M. Danish, Support vector regression (SVR)-based adsorption model for Ni(II) ions removal, Groundwater Sustainable Dev., 9 (2019) 100232, doi: 10.1016/j.gsd.2019.100232.
[24] M.H. Ahmadi Azqhandi, M. Ghaedi, F. Yousefi, M. Jamshidi, Application of random forest, radial basis function neural networks and central composite design for modeling and/or optimization of the ultrasonic assisted adsorption of brilliant green on ZnS-NP-AC, J. Colloid Interface Sci., 505 (2017) 278–292.
[25] N.M. Mahmoodi, J. Abdi, M. Taghizadeh, A. Taghizadeh, B. Hayati, A.A. Shekarchi, M. Vossoughi, Activated carbon/metal-organic framework nanocomposite: preparation and photocatalytic dye degradation mathematical modeling from wastewater by least squares support vector machine, J. Environ. Manage., 233 (2019) 660–672.
[26] H.-A. Tayebi, M. Ghanei, K. Aghajani, M. Zohrevandi, Modeling of reactive orange 16 dye removal from aqueous media by mesoporous silica/crosslinked polymer hybrid using RBF, MLP and GMDH neural network models, J. Mol. Struct., 1178 (2019) 514–523.
[27] S. Yildiz, Artificial neural network (ANN) approach for modeling Zn(II) adsorption in batch process, Korean J. Chem. Eng., 34 (2017) 2423–2434.
[28] H. Koyuncu, A.R. Kul, N. Yıldız, A. Çalımlı, H. Ceylan, Equilibrium and kinetic studies for the sorption of 3-methoxybenzaldehyde on activated kaolinites, J. Hazard. Mater., 141 (2007) 128–139.
[29] A.R. Kul, N. Caliskan, Equilibrium and kinetic studies of the adsorption of Zn(II) ions onto natural and activated kaolinites, Adsorpt. Sci. Technol., 2 (2009) 85–105.
[30] A.M. Ghaedi, A. Vafaei, Applications of artificial neural networks for adsorption removal of dyes from aqueous solution: a review, Adv. Colloid Interface Sci., 245 (2017) 20–39.
[31] X. Zhu, X. Wang, Y.S. Ok, The application of machine learning methods for prediction of metal sorption onto biochars, J. Hazard. Mater., 378 (2019) 120727, doi: 10.1016/j.jhazmat.2019.06.004.
[32] A. Jenkins, V. Gupta, M. Lenoir, General regression neural networks, radial basis function neural networks, support vector machines, and feedforward neural networks, Systems Control, arXiv:1911.07115 (2019) 1–4.
[33] C. McCormick, Radial Basis Function Network (RBFN) Tutorial, 2020. Available at: https://mccormickml.com/2013/08/15/radial-basis-function-network-rbfn-tutorial/ (Available: 01.01.2020).
[34] A.P. de M. Ramos Soares, F. de O. Carvalho, C.E. de Farias Silva, A.H. da Silva Gonçalves, A.K. de Souza Abud, Random forest as a promising application to predict basic-dye biosorption process using orange waste, J. Environ. Chem. Eng., 8 (2020) 103952, doi: 10.1016/j.jece.2020.103952.
[35] M. Awad, R. Khanna, Efficient Learning Machines: Theories, Concepts, and Applications for Engineers and System Designers, Apress, 2015, pp. 1–268.
[36] T. Kleynhans, M. Montanaro, A. Gerace, C. Kanan, Predicting top-of-atmosphere thermal radiance using MERRA-2 atmospheric data with deep learning, Remote Sens., 9 (2017) 1–16, doi: 10.3390/rs9111133.
[37] H. Pham, A new criterion for model selection, Mathematics, 7 (2019) 1215, doi: 10.3390/math7121215.
[38] E.O. Chijioke, T.N. Joseph, E.O. Paschal, O.A. Christian, Comparative analysis of RSM, ANN and ANFIS and the mechanistic modeling in eriochrome black-T dye adsorption using modified clay, S. Afr. J. Chem. Eng., 36 (2021) 24–42.
[39] M. Ghaedi, E. Shojaeipour, A.M. Ghaedi, R. Sahraei, Isotherm and kinetics study of Malachite green adsorption onto copper nanowires loaded on activated carbon: artificial neural network modeling and genetic algorithm optimization, Spectrochim. Acta, Part A, 142 (2015) 135–149.
[40] B. Beigzadeh, M. Bahrami, M.J. Amiri, M.R. Mahmoudi, A new approach in adsorption modeling using random forest regression, Bayesian multiple linear regression, and multiple linear regression: 2,4-D adsorption by a green adsorbent, Water Sci. Technol., 82 (2020) 1586–1602.
[41] M. Ghaedi, A.M. Ghaedi, E. Negintaji, A. Ansari, A. Vafaei, M. Rajabi, Random forest model for removal of bromophenol blue using activated carbon obtained from *Astragalus bisulcatus* tree, J. Ind. Eng. Chem., 20 (2014) 1793–1803.
[42] M.R.R. Kooh, M.K. Dahri, L.B.L. Lim, Jackfruit seed as low-cost adsorbent for removal of Malachite green: artificial neural network and random forest approaches, Environ. Earth Sci., 77 (2018) 1–12, doi: 10.1007/s12665-018-7618-9.
[43] A.R. Tehrani-Bagha, H. Nikkar, N.M. Mahmoodi, M. Markazi, F.M. Menger, The sorption of cationic dyes onto kaolin: kinetic, isotherm and thermodynamic studies, Desalination, 266 (2011) 274–280.
[44] A.A. Dil, A. Vafaei, A.M. Ghaedi, M. Ghaedi, E.A. Dil, Multi-responses optimization of simultaneous adsorption of methylene blue and Malachite green dyes in binary aqueous system onto Ni: FeO(OH)-NWs-AC using experimental design: derivative spectrophotometry method, Appl. Organomet. Chem., 32 (2018) 1–13.
[45] E.-K. Guechi, O. Hamdaoui, Sorption of Malachite green from aqueous solution by potato peel: kinetics and equilibrium modeling using non-linear analysis method, Arabian J. Chem., 9 (2011) 416–424.
[46] F. Mashkoor, A. Nasar, Preparation characterization and adsorption studies of the chemically modified *Luffa aegyptica* peel as a potential adsorbent for the removal of Malachite green from aqueous solution, J. Mol. Liq., 274 (2019) 315–327.
[47] T. Santhi, S. Manonmani, V.S. Vasantha, Y.T. Chang, A new alternative adsorbent for the removal of cationic dyes from aqueous solution, Arabian J. Chem., 9 (2016) 466–474.
[48] A.S. Sartape, A.M. Mandhare, V.V. Jadhav, P.D. Raut, M.A. Anuse, S.S. Kolekar, Removal of Malachite green dye from aqueous solution with adsorption technique using *Limonia acidissima* (wood apple) shell as low cost adsorbent, Arabian J. Chem., 10 (2014) 3229–3238.
[49] M. Mohammad, S. Maitra, B.K. Dutta, Comparison of activated carbon and physic seed hull for the removal of Malachite green dye from aqueous solution, Water Air Soil Pollut., 229 (2018) 1–14.
[50] S. Chowdhury, R. Mishra, P. Saha, P. Kushwaha, Adsorption thermodynamics, kinetics and isosteric heat of adsorption of Malachite green onto chemically modified rice husk, Desalination, 265 (2011) 159–168.
[51] S. Rangabhashiyam, P. Balasubramanian, Performance of novel biosorbents prepared using native and NaOH treated *Peltophorum pterocarpum* fruit shells for the removal of Malachite green, Bioresour. Technol. Rep., 3 (2018) 75–81.
[52] S. Chowdhury, P. Saha, Sea shell powder as a new adsorbent to remove Basic Green 4 (Malachite green) from aqueous solutions: equilibrium, kinetic and thermodynamic studies, Chem. Eng. J., 164 (2010) 168–177.
[53] L. Tian, J. Zhang, H. Shi, N. Li, Q. Ping Adsorption of Malachite green by diatomite: equilibrium isotherms and kinetic studies, J. Dispersion Sci. Technol., 37 (2016) 1059–1066.
[54] B.H. Hameed, M.I. El-Khaiary, Malachite green adsorption by rattan sawdust: isotherm, kinetic and mechanism modeling, J. Hazard. Mater., 159 (2008) 574–579.
[55] M. Zhang, Y. Mao, W. Wang, S. Yang, Z. Song, X. Zhao, Coal fly ash/$CoFe_2O_4$ composites: a magnetic adsorbent for the removal of Malachite green from aqueous solution, RSC Adv., 6 (2016) 93564–93574.
[56] M. Benjelloun, Y. Miyah, G.A. Evrendilek, F. Zerrouq, S. Lairini, Recent advances in adsorption kinetic models: their application to dye types, Arabian J. Chem., 14 (2021) 1–24.
[57] M.T. Yagub, T.K. Sen, S. Afroze, H.M. Ang, Dye and its removal from aqueous solution by adsorption: a review, Adv. Colloid Interface Sci., 209 (2014) 172–184.
[58] A.S. Eltaweil, H. Ali Mohamed, Eman M. Abd El-Monaem, G.M. El-Subruiti, Mesoporous magnetic biochar composite for enhanced adsorption of Malachite green dye: characterization, adsorption kinetics, thermodynamics and isotherms, Adv. Powder Technol., 31 (2020) 1253–1263.